Polarity-sensitive transient patterned state in a twisted nematic liquid crystal driven by very low frequency fields

K. S. Krishnamurthy,[1,*] Pramoda Kumar,[2] and M. Vijay Kumar[1]
[1]*Centre for Soft Matter Research, P.O. Box 1329, Jalahalli, Bangalore 560013, India*
[2]*Department of Physics of Complex Systems, Weizmann Institute of Science, Rehovot 76100, Israel*
(Received 5 December 2012; revised manuscript received 21 January 2013; published 15 February 2013)

We report, for a rodlike nematic liquid crystal with small positive dielectric and conductivity anisotropies, and in the 90°-twisted configuration, low frequency (<2 Hz) square wave electric field generated Carr-Helfrich director modulation appearing transiently over a few seconds at each polarity reversal and vanishing almost completely under steady field conditions. Significantly, the instability is polarity sensitive, with the maximum distortion localized in the vicinity of the negative electrode, rather than in the midplane of the layer. This is revealed by the wave vector alternating in the two halves of the driving cycle between the alignment directions at the two substrates. Besides the Carr-Helfrich mechanism, quadrupolar flexoelectric polarization arising under electric field gradient is strongly indicated as being involved in the development of the transient periodic order. Similar transient instability is also observed in other nematic compounds with varying combinations of dielectric and conductivity anisotropies, showing its general nature. The study also deals with various characteristics of the electro-optic effect that emerge from the temporal variation of optical response for different driving voltages, frequencies, and temperatures.

DOI: 10.1103/PhysRevE.87.022504 PACS number(s): 61.30.Gd, 47.54.−r, 47.52.+j, 47.20.Lz

I. INTRODUCTION

A strain-free nematic is invariant with respect to an inversion of its director, $\mathbf{n}\rightarrow-\mathbf{n}$. Curvature deformations of the splay and bend type break this symmetry, rendering the medium compatible with a polar order. The resulting flexoelectric ("flexo-," for short) polarization $\mathbf{P}_f$, which may be of dipolar [1] or quadrupolar [2] origin, is expressible as $\mathbf{P}_f = e_s\,\mathbf{n}(\nabla\cdot\mathbf{n}) + e_b(\nabla\times\mathbf{n})\times\mathbf{n}$, where e_s and e_b are the splay and bend flexocoefficients, respectively. In the converse flexoeffect, an applied electric field $\mathbf{E}$ induces curvature strains that generate the bulk flexotorque $\mathbf{\Gamma}_f = \mathbf{n}\times[(e_s - e_b)(\mathbf{E}\nabla\cdot\mathbf{n} - \nabla\mathbf{n}\cdot\mathbf{E}) + (e_s + e_b)\mathbf{n}\cdot\nabla\mathbf{E}]$ [3]. Here, the term involving $(e_s - e_b)$ is relevant for the flexoeffect due to director gradients in a homogeneous electric field [4,5]; the other involving $(e_s + e_b)$ is responsible for the gradient flexoeffect (GFE) due to an inhomogeneous electric field [2,6–8]. The flexoeffect due to the $(e_s - e_b)$ term in planarly aligned and strongly anchored thin samples was first explained by Bobylev and Pikin (BP) [4] as the volume instability, involving periodic polar and azimuthal angle distortions. It manifests optically as equidistant parallel stripes along the initial director. In a 90°-twisted nematic (TN) layer with the substrate easy axes along x and y, one might thus expect the BP domains to be diagonal, running along the initial midplane director $\mathbf{n}_{om}$. Detailed theoretical and experimental studies, however, show that the domains form at a slight angle to $\mathbf{n}_{om}$; while the magnitude of this angle depends on dielectric and elastic anisotropies, its sign reverses with the field direction [9,10]. As for the GFE, Derzhanski *et al.* [6] were the first to analyze it for a planar nematic in a static field, and predict its patterned and unpatterned modes; the former reveals optically as parallel stripes, again along the initial director, but it is characterized by only a periodic tilt modulation [7]. There have been subsequent experiments demonstrating morphologically similar, polarity-sensitive GFE domains [11]. There does not appear to be any study of the role of GFE in a nematic twist cell.

Nematics may bifurcate into quite a different patterned state, driven by the Carr-Helfrich (CH) mechanism [5,12]. For planar nematics with the initial director $\mathbf{n}_o = (1, 0, 0)$, in a dc field $\mathbf{E} = (0, 0, E)$, the CH analysis of the coupling between electrical conductivity anisotropy and the bend curvature distortion leads to periodic space charges of alternating sign appearing along the alignment direction, x. The body force on these charges sets up periodic cellular flows above a critical voltage V_c determined by the balance between hydrodynamic, dielectric, and elastic torques. Optically, this nonequilibrium dissipative roll instability appears as periodic focal lines parallel or slightly inclined to the normal to $\mathbf{n}_o$. In a 90°-TN layer, where largely normal rolls are predicted [13], one might expect the wave vector $\mathbf{q}$ of the roll pattern to be along $\mathbf{n}_{om}$. However, as in the case of the BP mode, under dc excitation, $\mathbf{q}$ is found to be slightly oblique relative to $\mathbf{n}_{om}$ and also polarity sensitive [14].

This study concerns the coupling between flexoeffect and electroconvection in a 90°-twisted nematic sample excited by very low frequency square wave fields. In earlier analyses of this coupling, flexoterms involving both $(e_s - e_b)$ and $(e_s + e_b)$ have been considered [15–19]; however, the field inhomogeneity taken into account is primarily that of the transverse electric field due to space charges, and the time dependent spatial gradients along the applied field are ignored. From our results, the latter emerge as quite significant in low frequency experiments. In particular, we find patterned states in which the wave vector selection is polarity determined and the low frequency distortion, instead of originating in the sample midregion, is confined to the immediate neighborhood of the negative electrode. Further, the CH mode is activated

*Author to whom correspondence should be addressed: murthyksk@gmail.com, murthyksk@csmr.res.in

transiently at voltage sign reversals and is suppressed under steady field conditions. These observations indicate that, in the development of low frequency transient instabilities, GFE plays a key role, and that electrode polarization of ionic origin is too important to be ignored. It is our purpose here to present and discuss these observations. Our studies are particularly relevant in the light of recent findings on competing BP and CH modes in nematics driven by very low frequency (f) fields [20–22]. For example, it is predicted that the limit $f \to 0$ is singular and that the periodic modulations characteristic of these two instabilities occur one after the other, in bursts, in each half of the low frequency driving cycle. Observations on a planar nematic (Phase 5, Merck) driven by sine wave fields are found to be in consonance with these predictions [21,22]. While the transient appearance of the CH instability may thus be understood, its localization near an electrode as observed here does not emerge from the present theory [20].

II. EXPERIMENTS

We used a reagent grade sample of butyl 4-(4-ethoxyphenoxycarbonyl) phenyl carbonate (BEPC) supplied by Eastman Organic Chemicals. It exhibited an enantiotropic nematic phase

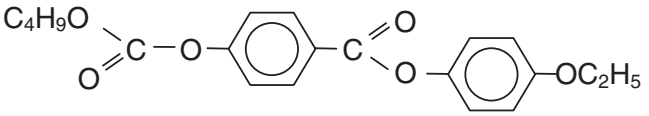

between ~55 °C and 84 °C. The sample cells used were sandwich type, constructed of indium tin oxide (ITO) coated glass plates. Planar anchoring was secured by spin coating the ITO electrodes with polyimide (PI-2555 from HD Microsystems), curing at 270 °C for 1 h, and then buffing unidirectionally the coated surfaces on a tissue paper. The rubbing directions at the two substrates and the layer normal define the reference axes (x, y, z), as indicated in Fig. 1 depicting the sample geometry. Mylar spacers, heat-sealed to the electrodes through cooling from ~250 °C under a uniform pressure, determined the cell gap, which was measured interferometrically. For optical observations, a

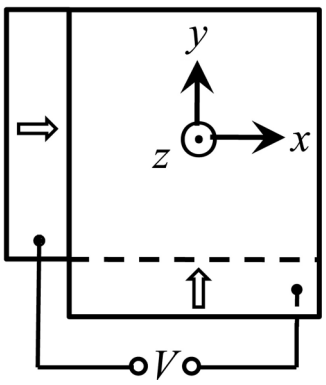

FIG. 1. Sample configuration for observing the instabilities in a 90°-twisted nematic layer of BEPC. Block arrows indicate the rubbing directions at the substrates. Applied field along z is taken to be positive. V denotes the applied dc or rms ac voltage. Light is incident along z.

Carl-Zeiss Axio Imager.M1m polarizing microscope equipped with an AxioCam MRc5 digital camera was used. The sample temperature T was maintained to an accuracy of ± 0.1 °C by an Instec HCS402 hot stage connected to a STC200 temperature controller. The voltage source was a Stanford Research Systems DS345 function generator coupled to a FLC Electronics voltage amplifier (model A800). The applied voltage was measured with a Keithley-2002 multimeter. We employed a photodiode (Hamamatsu S2281) with a wideband amplifier (Hamamatsu C9329) for transmitted light intensity measurements; the selected amplifier photosensitivity was 10^9 V/A. For data storage and display, we used a PC-based digital oscilloscope (PicoScope 4262).

For BEPC, the value of permittivity anisotropy $\varepsilon_a = \varepsilon_\parallel - \varepsilon_\perp$ (the subscripts $\parallel$ and $\perp$ referring to directions relative to the nematic director) is reported to vary from 0.21 at the melting temperature to 0.06 at 84 °C [23]. The results of our independent dielectric measurements on BEPC agreed with the reported data to within 5%. For fresh samples of BEPC, electrical conductivity $\sigma_\perp$ varied between 6.85×10^{-8} S m^{-1} at 55 °C and 19.25×10^{-8} S m^{-1} at 75 °C; also, $\sigma_\parallel/\sigma_\perp$ decreased from 1.25 at 55 °C to 1.19 at 75 °C. The birefringence of BEPC ranges from 0.141 at 56 °C to 0.087 at 83 °C [24].

For convenience, the polarizer-analyzer setting will be represented as P(α) − A(β), where α and β are the angles in degrees relative to the x direction.

III. RESULTS AND DISCUSSION

A. Field induced stationary director distortion states

Before taking up the very low frequency effects that form the main focus of this paper, for later comparison, it is useful to deal with the instabilities in the frequency regime above 2 Hz. The phase diagram of BEPC, in the voltage-frequency (V-f) plane, under excitation by a square wave field of frequency in the range 2–350 Hz, is presented in Fig. 2. Here V_{OF} is the optically determined Fréedericksz threshold corresponding to the onset of a uniform change in the birefringence color of the base state as illustrated in Figs. 2(a) and 2(b). V_{OF} is expected to be slightly higher than the actual threshold V_F from cell capacitance measurements. In planar cells of BEPC, V_{OF} is found to be ~9% more than V_F [25]. Theoretically, for a 90° twist cell, V_F is given by

$$V_F = \frac{\pi}{2}\sqrt{\frac{4k_{11} - 2k_{22} + k_{33}}{\varepsilon_o \varepsilon_a}}. \quad (1)$$

Here k_{11}, k_{22}, and k_{33} are the splay, twist, and bend elastic moduli, respectively, and ε_o is the free space permittivity. Evidently, V_F is expected to be independent of frequency in the static permittivity region, well below the onset of dielectric relaxation. We found V_{OF} to remain almost constant from 10 kHz to about 350 Hz. However, for lower frequencies, as depicted in Fig. 2, a marginal steady decrease in V_{OF} is observed. This result is surprising in terms of the theory of dielectric alignment in conducting nematics [26], which predicts, for a planar sample, the same threshold $V_F = \pi[k_{11}/(\varepsilon_o \varepsilon_a)]^{1/2}$ as for the nonconducting case, but an altered distortion amplitude or

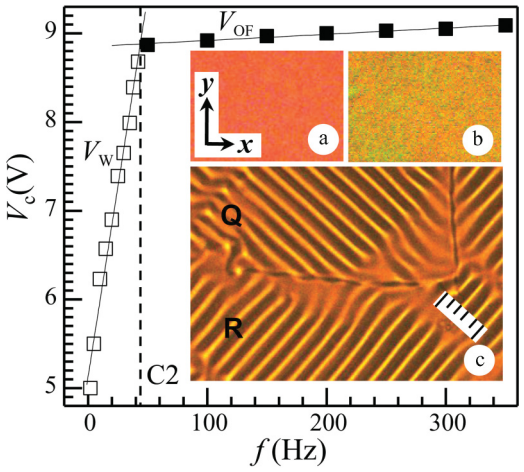

FIG. 2. (Color online) Critical voltage V_c for the onset of primary instability as a function of frequency f of the applied square wave field. V_W and V_{OF} denote the optical thresholds for Williams roll and Fréedericksz bifurcations, respectively. $V_W(f)$ and $V_{OF}(f)$ curves intersect at the codimensional point C2. Insets: (a) interference color for P(45)–A(45) in the field free state at 55 °C; (b) Fréedericksz state, slightly above threshold, 350 Hz, 9.09 V; (c) focal lines due to Williams rolls at $\pm 45°$ to x, in reverse quarter-turn twisted regions Q and R separated by an L-shaped disclination; 15.6-μm-thick sample; 20 Hz, 7.28 V, 55 °C, A(90), 10 μm each scale division.

maximum midplane tilt θ_M given by

$$\frac{V}{V_F} = 1 + \frac{\theta_M^2}{4}\left(1 + \frac{k_{33} - k_{11}}{k_{11}} + a\right) + O\left(\theta_M^4\right) + \cdots, \quad (2)$$

where

$$a = \left[\frac{\sigma_a}{\sigma_\perp} + \left(\frac{f}{f_q}\right)^2 \frac{\varepsilon_a}{\varepsilon_\perp}\right]\left[1 + \left(\frac{f}{f_q}\right)^2\right]^{-1}.$$

Here, the charge relaxation frequency, $f_q = \sigma_\perp/(2\pi\varepsilon_o\varepsilon_\perp)$. Thus V_{OF} corresponding to a given θ_M at which the birefringence color begins to change may be expected to be linear in a. For the anisotropic electrical parameters of BEPC at 55 °C, we find $a(f)$ to be quite linear and given by $a = 0.2645–5.0984\times10^{-4} f$. In other words, assuming the validity of Eq. (2) for the TN case here, we would expect V_{OF} to increase with lowering frequency, contrary to our result. This conclusion is not reversed even if the value of $\sigma_\perp$ is doubled, keeping σ_a unchanged; only on simultaneously changing $\sigma_a/\sigma_\perp$ from 0.25 to about 0.039 will the trend reverse. It is, therefore, unlikely that possible conductivity changes during extended electric field experiments are responsible for the observed $V_{OF}(f)$ trend. What the theory [26] does not consider is the surface polarization of ionic origin, which could affect the anchoring [27,28]. Similarly, flexoelectric polarization of quadrupolar origin could influence the dielectric response [29–31]. Conceivably, the frequency dependence of these effects could account for the observed $V_{OF}(f)$ trend.

The optical threshold V_W of the CH instability [12,32–35], which corresponds to the appearance of focal lines due to the Williams roll instability, is linear in f (Fig. 2). While this is only to be expected in the high frequency region, a nonlinear scaling of V_W, roughly as $\sqrt{1 + (f/f_q)^2}$ when $\varepsilon_a \ll 1$, is predicted at lower frequencies [33,34,36]. By implication, $V_W(f)$ should show a vanishing slope toward the dc limit. More specifically, for BEPC at 55 °C ($f_q = 228$ Hz), between the C2 frequency f_{C2} and 2 Hz, V_W should drop by only about 1.9% of its value at f_{C2}; however, the drop seen in Fig. 2 is by as large as 44% of $V_W(f_{C2})$. In other words, the observed behavior in the low f regime indicates a lowering of the threshold, compared to its theoretical value, by a quantity that increases continuously with decreasing f. This is likely to be again due to flexoelectric influence prominent at very low frequencies. In fact, for a static field acting on an initially planar layer, the theoretical finding is that the flexoelectric effect reduces the electroconvection (EC) threshold [15–17]. More recently, a similar effect has also been predicted for ac fields [18,19], with the flexoelectric influence decreasing progressively on increasing f.

Morphologically, as seen in inset (c) of Fig. 2, the CH rolls form at $\pm 45°$ to x, in reverse twisted regions. The corresponding wave vectors in these regions lie along the easy axes in the layer middle, where it may be expected that the substrate anchoring effect is the least and, therefore, the field induced distortion, the largest [37]. It may be noted here that the Lifshitz frequency, below which oblique rolls form at threshold, is predicted to decrease with increasing twist and decreasing σ_a; in consequence, when the twist angle is 90° and σ_a is low, as in the present case, only the normal roll state is possible [13]. As the frequency is reduced, the diagonal disposition of the pattern wave vector is not seriously affected until about 2 Hz. However, the threshold pattern becomes more and more localized with lowering f. In Fig. 3 illustrating this effect for $f = 2$ Hz, the focal lines are confined to parallel bands separated by structureless regions. Adjacent focal lines in a band are splayed out, with one of the lines toward x and the other toward y. The pattern is highly time dependent, decaying continuously in one region, while evolving in another. In addition, the focal lines in a band are oscillatory about the diagonal and also propagative at threshold. The latter instability (Hopf bifurcation), explicable by the weak electrolyte model [34] that assumes the existence of two mobile ionic species, is found almost throughout the

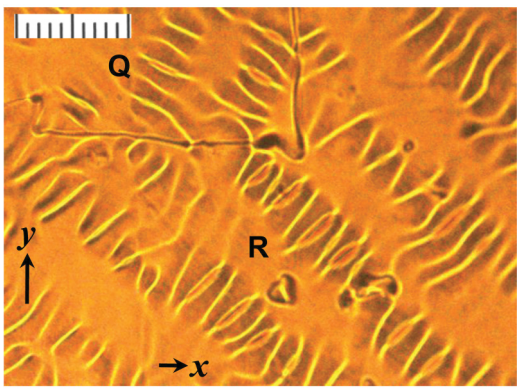

FIG. 3. (Color online) Patterned bands of focal lines in reverse quarter-turn twisted regions Q and R separated by an L-shaped disclination; the focal lines run at about $\pm 45°$ to x on the average, with adjacent lines in a band splayed out; 15.6-μm-thick sample, 2 Hz, 5.0 V, 55 °C; A(90), 10 μm each scale div.

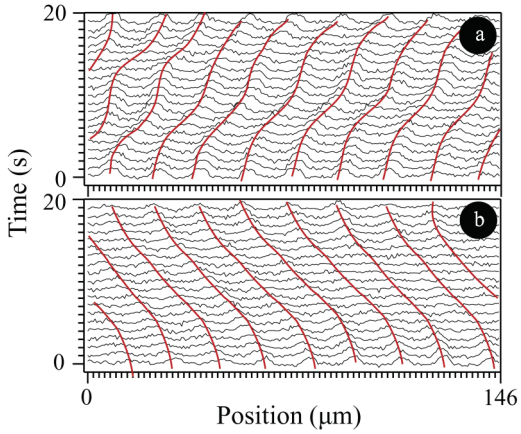

FIG. 4. (Color online) Profiles of transmitted light intensity along a fixed diagonal line parallel to the local wave vector in the time images; successive profiles along the vertical are separated by 1 s. The constant phase thick lines in brown are not straight due to quasiperiodic fluctuations in intensity of focal lines. Plots (a) and (b) correspond to two of the contiguous regions along the stripe direction with opposite drift velocities. The average drift speed is about 0.9 μm s^{-1} in (a) and 1.1 μm s^{-1} in (b); 7.08 V, 55 °C.

regime of electroconvection in Fig. 2. In Fig. 4, we demonstrate the opposite drifts present in two adjacent patterned bands of the sample under excitation by a 20 Hz field.

B. Field induced periodically modulated transient state

On sudden application of a sufficiently large static voltage (∼8 V) across a twisted nematic layer of BEPC, the structureless base state gets momentarily destabilized by a patterned state. The effect manifests optically as a periodic array of focal lines appearing briefly under unsteady conditions. The corresponding director distortion grows rapidly to its maximum in a fraction of a second and then decays over a few seconds toward its eventual disappearance. The optical characteristics of the transient line images are the same as of normal rolls of the CH instability. When using a single polarizer, for example, they are seen with maximum visibility for the incident light vibrating parallel to the easy axis x at the entrance substrate, and they are not revealed when the transmission axis of the polarizer is set along y. Similarly, the pattern of parallel line images, with an average period of $\sim 2d$, is seen in a succession of real and virtual focal planes on either side of the $z = 0$ midplane of the layer. A significant feature of the patterned state, which is the central theme of this report, concerns its wave vector direction. It is polarity sensitive, being along y or x depending, respectively, on whether the electric field is positive or negative. In other words, the line images form along x when the bottom electrode in Fig. 1 is positive, and they form along y when this polarity turns negative. Therefore, the periodic splay-bend distortion responsible for modulation of the extraordinary index does not originate in the layer midplane as is usually supposed. On the contrary, it is confined to the close neighborhood of the negative electrode.

The foregoing observations on the transiently existing patterned electroconvective state are best illustrated with reference to the instabilities driven by a low frequency square wave

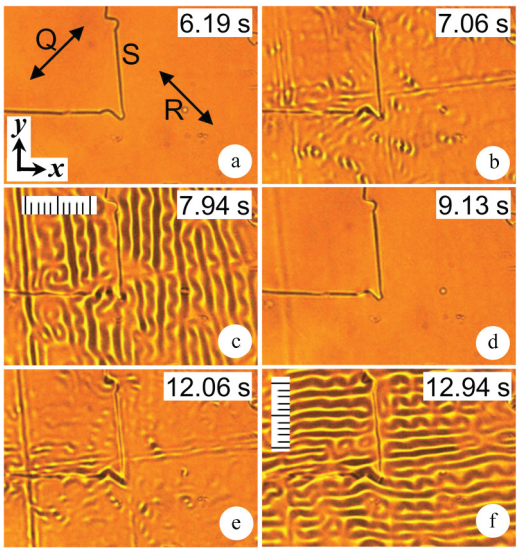

FIG. 5. (Color online) Transient switching into a patterned state during polarity reversals of a square wave field of frequency 0.1 Hz and voltage amplitude 3.15 V, observed in a 15.6-μm-thick layer at 55 °C. (a)–(f) Snapshots from a time series, with time stamps showing the recording time relative to start of the series; P(0), 10 μm each scale division. The average period of the patterns in (c) and (f) is about $2d$; in (c) and (f), the wave vectors are along the alignment directions at the bottom and top substrates, respectively; in (c) the field is along $-z$ after switching; it is the reverse in (f). Q and R are reverse twisted regions separated by a disclination line S of strength 1/2; double-headed arrows within these regions indicate the midplane alignments; Q is right-handed and R left-handed.

field, as in Fig. 5. The snapshots here are from a time image series recorded with a 15.6-μm-thick sample at 55 °C, exposed to a square wave field of frequency 0.1 Hz and voltage amplitude 3.15 V. Figures 5(a) and 5(d) show the patternless base state shortly before polarity reversal, when the field is steady. In Figs. 5(c) and 5(f), each showing the texture shortly after polarity switching, the wave vectors are along the alignment directions at the bottom and top substrates, respectively. In Fig. 5(c), the field is along $-z$ after switching; it is the reverse in Fig. 5(f). Notably, for both the reverse twisted regions Q and R, the pattern wave vector remains the same for a given field direction. This is in contrast to the situation in Fig. 2(c), where the image lines in reverse twisted regions are nearly orthogonal, running diagonally at $\pm 45°$ with respect to x.

The evanescent occurrence of distortion is also evident from a concomitant change in transmitted light intensity. With our experimental setup, it was possible to notice a change in transmission level at each polarity switching for even as low a potential drop as 1.0 V at 0.1 Hz, as exemplified in Fig. 6. The differential optical response, or the degree of distortion, for opposite field directions, as seen in Figs. 6(b) and 6(c), is a reflection of slightly dissimilar conditions prevailing at the two substrates. For excitation voltages above ∼2 V, the distortion becomes more extended and discernibly periodic; correspondingly, the optical response improves a great deal, as evident in Fig. 7. It is clear from the intensity of peaks in Fig. 7(b) that the distortion decays substantially, by over 90%, in about 4 s, while the subsequent relaxation proceeds

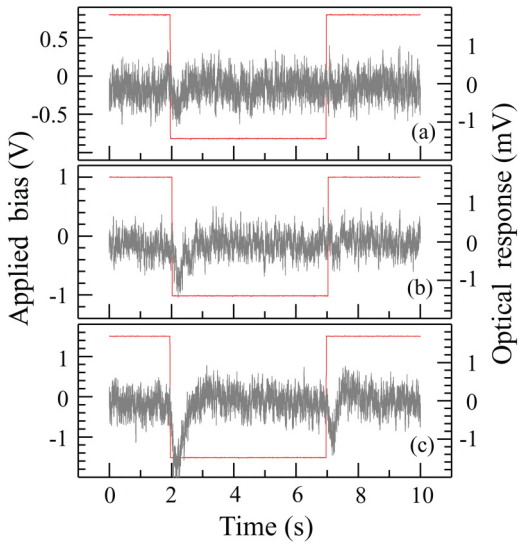

FIG. 6. (Color online) Transient director distortion occurring at field polarity reversals as observed at low bias voltages using a PicoScope, ac coupled to the transimpedance amplifier. (a) For $V = 0.8$ V, the optical signal is practically buried in the background; (b) for $V = 1.0$ V, a weak transmittance switching is discerned, but only at the first polarity change, at $t \sim 2$ s; (c) For $V = 1.5$ V, momentary change in transmittance follows each field reversal; 77 °C.

asymptotically until its disruption at the next polarity change. The shape of transmission profile for a given bias is dependent on temperature or the initial phase difference in the field free state, $\delta_o = 2\pi d(n_e - n_o)/\lambda$, where $(n_e - n_o) = \Delta n$ is the birefringence for wavelength λ. Before elaborating this point, we may first consider the transmission profile under varying temperature, in the absence of field. In a 90° twist cell, the optical modes are linearly polarized parallel and perpendicular to the nematic director, and follow the twist, provided the Mauguin condition $u = 2\Delta nd/\lambda \gg 1$ is fulfilled. In most of our experiments, $d = 15.6$ μm; reported data [24] on $\Delta n(T)$ for BEPC closely fit the equation $\Delta n = 0.075\,06(85.1936 - T)^{0.17811}$, with T in degrees Celsius. Thus, between 80 °C and

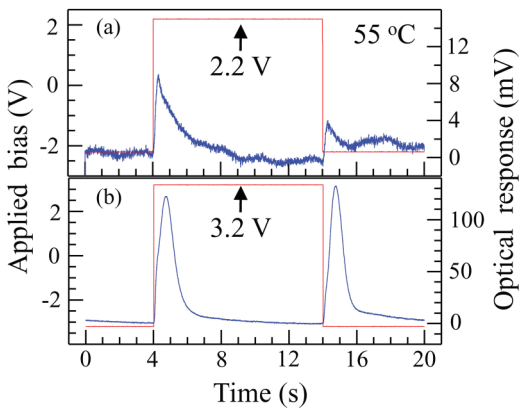

FIG. 7. (Color online) Electro-optic response in a 15.6-μm-thick twisted nematic layer of BEPC at 55 °C, driven by a 50-mHz square wave field of voltage amplitude 2.2 V (a) and 3.2 V (b). Each polarity reversal is followed by a transient sudden increase in transmitted light intensity. Parallel polarizers P(45)–A(45), mercury green light.

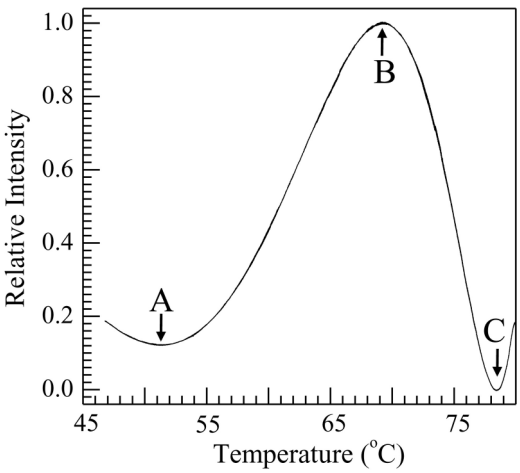

FIG. 8. Relative intensity of light transmitted from a 15.6-μm-thick, 90°-twisted BEPC layer, in the field free state, as a function of temperature. Parallel polarizers P(45)–A(45); mercury green light. The phase differences at A, B, and C are 8π, 7π, and 6π, respectively. The difference in relative intensities at A and C presumably arises from temperature dependent light scattering.

50 °C, u varies here between 5.75 and 8, and we may, therefore, take the sample as in the waveguide regime in the field free state. For a cell placed between parallel polarizers with their axes bisecting the angle between the alignment directions at the substrates, the transmittance τ in the field off state should vary as $\sin^2(\delta_o/2)$. Figure 8 shows the temperature variation of relative τ in BEPC for mercury green light. The maximum and minimum intensity positions here are as expected from the sample thickness and $\Delta n(T)$.

We may now discuss the shape of intensity profiles in the field on state. In Fig. 7, for example, a single transmission peak appears soon after switching. Before switching, the initial phase difference corresponding to 55 °C, as can be seen from Fig. 8, is slightly less than 8π. In the on state, during the transitory director distortion, the tilt angle θ is a function of x, z, and t. The excursion of its effective value θ^* from 0 to the maximum θ_M and back results in δ decreasing at first from δ_o to some value δ_M corresponding to the observed intensity maximum, and then increasing back to δ_o. Evidently, the applied bias of 3.2 V in Fig. 7(b) is insufficient for δ_M to fall below 7π. We show in Fig. 9 the electro-optic response for two other temperatures to illustrate the effect of δ_o on the appearance of transmission curves. At $T = 77$ °C, during each switching, the transmission rises to a peak between two minima, as at H between L_1 and L_2 in Fig. 9(a); by contrast, at 66 °C, the intensity falls to a minimum between two maxima, as at L between H_1 and H_2 in Fig. 9(b). These features are readily explained with reference to Fig. 8. For example, at 77 °C, δ_o is slightly above 6π; in the on state, when δ drops continuously to a value between 6π and 5π and then increases back to the initial value, the forward and reverse passages through 6π result in two transmission minima, at L_1 and L_2. It may be noted that, in Fig. 9, the optical response voltage is shown relative to the baseline at 0 mV. Experimentally, the baselines for different temperatures are in fact shifted in accordance with Fig. 8. This is shown in Fig. 10, giving the profiles for various temperatures, recorded at constant voltage

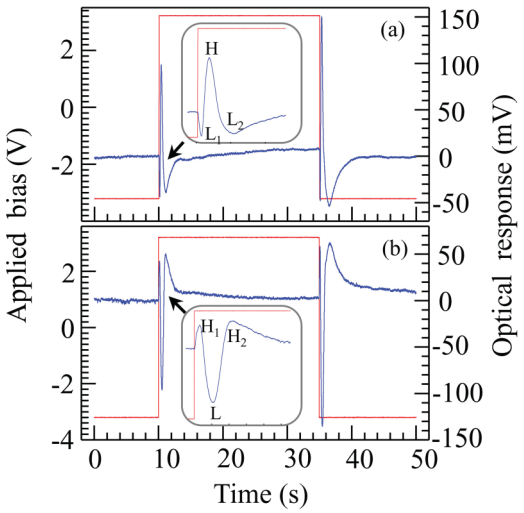

FIG. 9. (Color online) Electro-optic response in a 15.6-μm-thick twisted nematic layer of BEPC, driven by a 20-mHz, 3.2-V square wave field. (a) 77 °C, (b) 66 °C. Insets are regions indicated by arrows with time-scale enlargement to show the shape of the profiles. Each polarity reversal is followed by a transient sudden change in transmitted light intensity. Parallel polarizers P(45)–A(45); mercury green light.

and frequency. It may also be observed in Fig. 10 that the peak height relative to the minimum in each case is determined by the combination of initial birefringence and maximum distortion amplitude; the latter increases with temperature due to decreasing rotational viscosity.

The effect of applied voltage on optical response may be described, for example, with reference to Fig. 9(a). Here, the peak at H between L_1 and L_2 increases in intensity with V until saturation corresponding to $\delta \leqslant 5\pi$. When the maximum distortion corresponds to $4\pi < \delta < 5\pi$, we expect to observe two equal maxima that mark the transit of δ across 5π. In Fig. 11 presenting these characteristics, this intensity doublet is clearly indicated by the shoulder in the profile for 3.5 V; the two peaks are well resolved at 3.8 V. The transition from the single to double-peak region at about 3.5 V is also

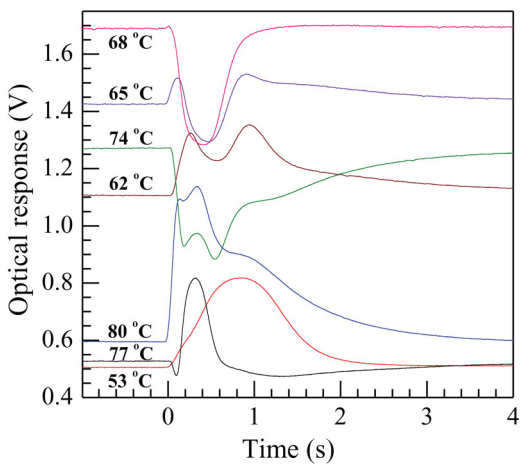

FIG. 10. (Color online) Effect of temperature on optical response for mercury green light, when the voltage and frequency of the driving square wave field are held constant.

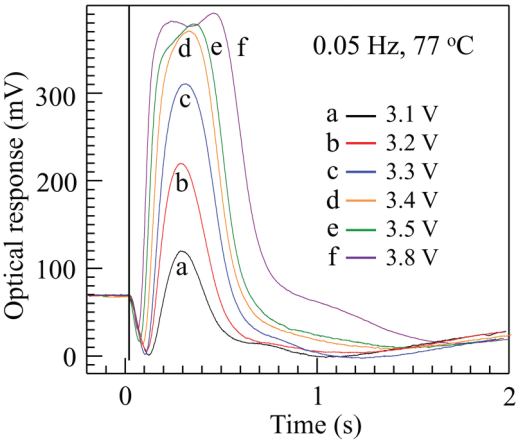

FIG. 11. (Color online) Electro-optic response in a 15.6-μm-thick sample of BEPC for various voltages of the driving square wave field. Switching time is indicated by the vertical dark line close to 0 s. Parallel polarizers P(45)–A(45); mercury green light.

indicated by voltage variation of the time interval at half maximum intensity relative to the minimum, as shown in Fig. 12. Thus, the peak optical response of ~380 mV for $V = 3.5$ V may be taken to correspond to the maximum transmittance ($\tau = 1$) while determining $\delta(t)$. We present in Fig. 13 the variation $\delta(t)$ corresponding to normalized τ as a function of t, at 3.15 V. Beyond 0.3 s, it nearly fits a double-sigmoid function represented by the continuous (red) line (Fig. 13); it is associated with three inflections, of which two occur in the narrow interval 0.6–1.2 s; the corresponding disruption of smooth relaxation at K in the inset, or shortly before the second minimum in Fig. 11, is possibly attributable to backflow effects. For example, in a 90°-twisted layer, after field turnoff, relaxation from a strongly distorted Fréedericksz state produces an oscillatory optical response, often described as the "bounce" in transmission [38]. It is a noninertial effect, essentially due to the hydrodynamic motion associated with director rotation, which in turn induces a reverse rotation of

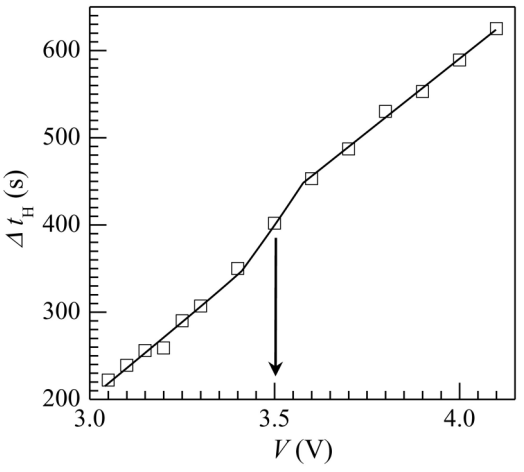

FIG. 12. Time interval at half the maximum intensity for peak H in Fig. 9(a), as a function of applied voltage. The transition between the two linear sections across 3.5 V corresponds to the phase difference crossover from $>5\pi$ to $<5\pi$.

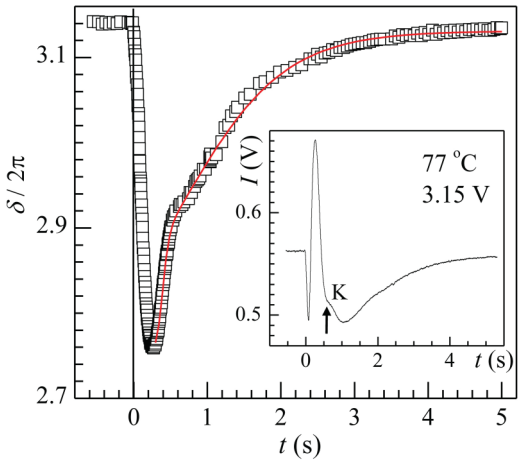

FIG. 13. (Color online) Time dependence of effective phase difference δ during the transient occurrence of the Carr-Helfrich instability following polarity reversal of the driving square wave field at $t = 0$ s; the $\delta(t)$ plot is for the transmitted intensity profile $I(t)$ (inset) recorded with $V = 3.15$ V. The continuous (red) line in the $\delta(t)$ plot is a double-sigmoid fit for the data in the time interval 0.3–5 s. To normalize the output voltage, the peak optical response of 380 mV at $V = 3.5$ V (see Fig. 11) is used. The disruption of smooth relaxation at K in the inset, shortly before reaching the second minimum, is attributable to backflow effects.

the molecules in the region of maximum distortion. A similar effect may be envisaged for the relaxing periodic distortion.

Frequency of the applied field has a considerable influence on the transient response. From Fig. 14 depicting the optical response as a function of time at various frequencies, it is readily seen that the peak intensity, which is a measure of distortion amplitude, is a decreasing, sigmoidlike function of f. In consequence, the positions of maximum and second minimum of intensity, which indicate the rise and decay delays, respectively, are shifted to lower times with increasing f. This may be interpreted as due to the dependence of V_c on f; for the usual CH instability, as f increases, V_c increases nonlinearly, leading

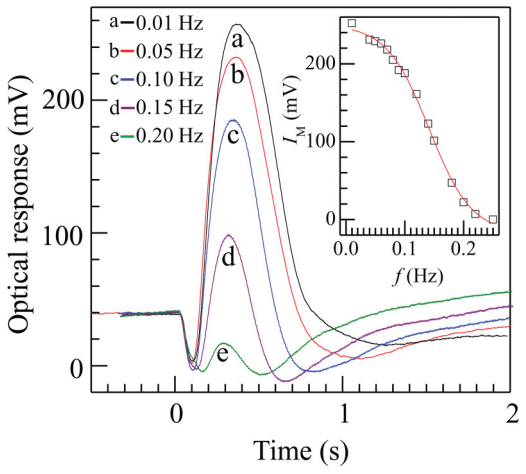

FIG. 14. (Color online) Effect of frequency on optical response for constant voltage of 3.4 V of the driving square wave field. Inset: Peak intensity I_M relative to the first minimum as a function of f. Continuous line is a sigmoidal fit; 3.4 V, 77 °C.

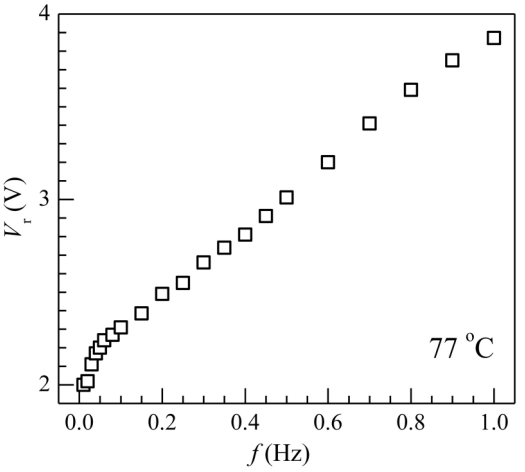

FIG. 15. Frequency variation of applied square wave voltage V_r at which the optical response is 10 mV.

to a decrease in the control parameter, $\varepsilon = (V^2/V_c^2) - 1$, corresponding to a given voltage. With a similar trend of $\varepsilon(f)$ here, the distortion amplitude would be expected to lower with elevation in f. As earlier noted, the threshold V_c is less well defined in our case due to the sensitivity of transient response to substrate conditions. On the other hand, the driving voltage V_r corresponding to a given optical response, which is accurately measurable, may be considered as a direct measure of the threshold. Figure 15 shows the frequency variation of V_r at which a response voltage of 10 mV is obtained. As expected, $V_r(f)$ is an increasing function which is almost linear above 50 mHz. The progressive dip toward the static limit below this frequency is possibly due to increasing flexoelectric influence [18,19].

The faster rise and decay of distortion for increasing frequency (Fig. 14) is also reflected in the frequency variation of t_{12}, the time interval between the first and second minima in the optical transmission profile. As shown in Fig. 16, t_{12} decreases exponentially with f. In effect, an increase in

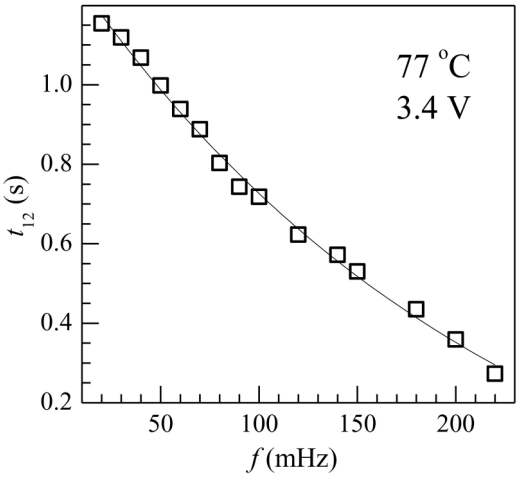

FIG. 16. Frequency variation of t_{12}, the time interval between the first and second minima in the optical transmission profile recorded using parallel polarizers P(45)–A(45) and incident mercury green light. The continuous curve is an exponential fit.

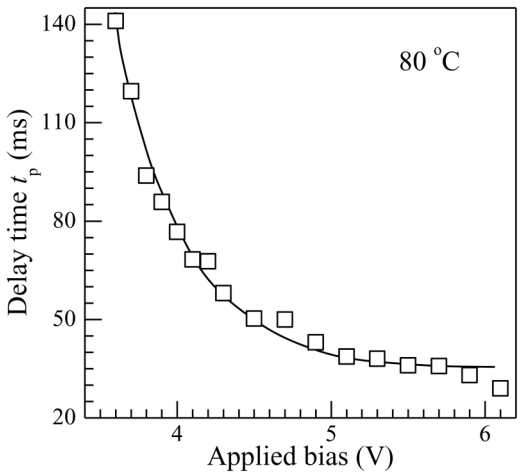

FIG. 17. Dependence on applied voltage of the time of occurrence t_p of peak transmission after polarity reversal. The continuous curve is an exponential fit.

frequency at a given driving field has a similar influence on the optical response as a decrease in field at a given frequency. This is illustrated in Fig. 17 where the time of occurrence t_p of peak transmission after polarity reversal decreases exponentially under increasing bias voltage. The decay of distortion, however, becomes slower with increasing bias. For instance, as exemplified in Fig. 18, the optical response at a given time, after a few seconds of polarity reversal, increases exponentially with V.

Under dc driving, below ~10 V, the quiescent state persists and the initial birefringence color shows little change, as illustrated in Figs. 19(a) and 19(b). On further elevation in V, reorientation becomes extensive well above the expected V_F; however, instead of a homogeneous change in birefringence color characteristic of the Fréedericksz state, an irregular stripes pattern evolves. The wave vector appears inclined more toward x when the field is negative or along $-z$, as in Figs. 19(c) and 19(d); it tends toward y for positive fields, as in Figs. 19(e) and 19(f). These results confirm the propensity

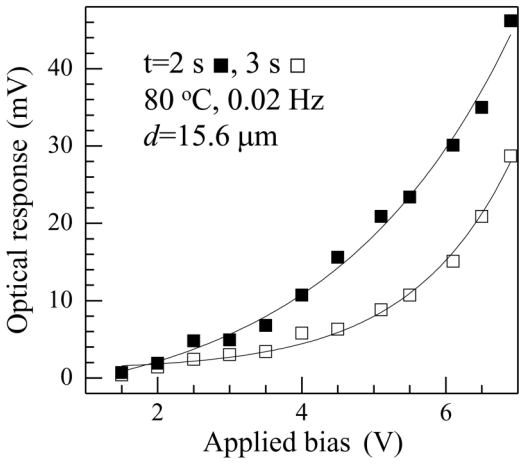

FIG. 18. Optical response during the decay of distortion, at times t after polarity reversal, as a function of applied voltage. Transmitted intensity in the absence of field (baseline) is taken to correspond to 0 mV. The continuous curves are exponential fits.

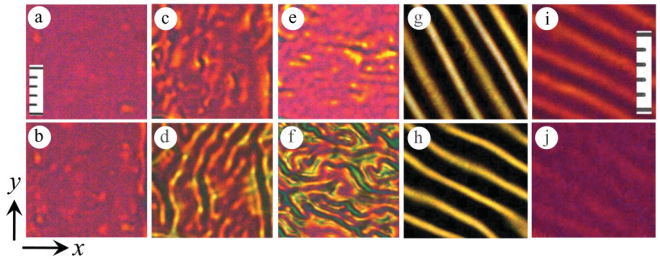

FIG. 19. (Color online) Distortions in a dc excited BEPC layer at 55 °C. (a)–(f) 8.9-μm-thick sample between ITO plates with a single coat of polyimide; −6 V (a), −10.6 V (b), −15 V (c), −17.4 V (d), 11.1 V (e), 17.4 V (f); P(45)–A(45); 5 μm each scale division; the birefringence color in (a) is almost the same as of the base state; the color change in (b) is marginal and inhomogeneous; the high voltage textures show irregular stripes that stretch principally along y in (c), (d), and along x in (e), (f). (g)–(j) 7.6-μm-thick sample between ITO plates with two coats of polyimide; −10 V (g), 10 V (h), 8 V (i), (j); frames (i) and (j) from time series are separated by 45 s; A(90) in (g), (h), P(45)–A(45) in (i), (j); 5 μm each scale division.

of periodic modulation to occur near the negative electrode rather than in the middle of the layer. The irregular buildup of periodic distortion, evident in Figs. 19(c)–19(f), is a result of incomplete blocking of charge injection. We draw this conclusion from the results of a dc field experiment on a sample sandwiched between two electrodes, each covered with a thick aligning film comprising two polyimide layers, applied and cured successively. In this case, even at 10 V, the patterns are clearly defined and well developed, as exemplified in Figs. 19(g) and 19(h). In fact, when increasing V gradually at 0.1 V s^{-1}, EC sets in definitively below V_F, at 8 V, as seen in Fig. 19(i); however, the distortion decays with time and eventually disappears as in Fig. 19(j). It is pertinent to add that the momentary appearance of EC at polarity reversals of a low frequency voltage remains unaffected under improved blocking of charge injection.

In order to check the generality of our above results, we have also examined low frequency field excited EC in 4,4′-diheptyloxyazoxybenzene (HOAB) and 4,4′-dimethoxyazoxybenzene (PAA, *p*-azoxyanisole). Whereas the sign combination of (ε_a, σ_a), in that order, is (+ +) for BEPC, it is (− −) for HOAB and (− +) for PAA. For nematics of the (− +) class, or (+ +) class and with a small ε_a, CH destabilization is readily described by the standard model that ignores the flexoelectric contribution to space charge density [33,34]. However, in (− −) nematics, EC is flexoelectrically stimulated [15–19]. We find the temporal EC phenomenon, such as exhibited by BEPC, in both HOAB and PAA. For illustration, the transient patterns for TN HOAB are presented in Fig. 20(a). In Fig. 20(b), for comparison, the temporal effects are shown for an untwisted planar HOAB sample.

C. Significance of transient evolution of periodic order

Between purely orientational BP and electroconvective CH phenomena, to which class does the transient periodic modulation in BEPC belong? From the wave vector direction along the x or y axis in twist cell experiments, of course, it is not possible to choose between the two modes. In addition, the momentary

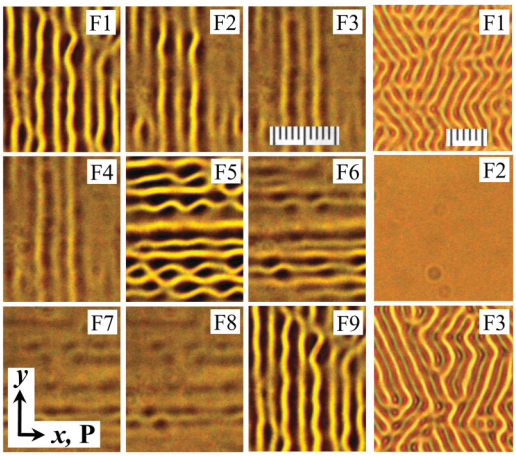

FIG. 20. (Color online) (a, columns 1–3) Transient evolution of vertical (Y) and horizontal (X) stripe states occurring at polarity reversals of a square wave field in a 90°-twisted, 8.3-μm-thick, nematic sample of HOAB at 122 °C; 2 μm each scale division; $f = 0.453$ Hz, $V = 5.1$ V. Frames F1–F9 are from time lapse recordings, with successive frames in the series separated by $T_F = 0.276$ s (corresponding to a frame rate $f_R = 3.623$ s^{-1}). Here $f = f_R/8$, so that frames recorded at successive polarity reversals (F1, F5, F9) are separated by three frames captured during field constancy (F2–F4 and F6–F8). The latter frames, which may be said to belong to the decay (D) state, show progressive relaxation of the Y or X state evolved previously. Note that, when $f = f_R$, all the images of the series display the same morphology, which may be patterned or unpatterned depending on the start time; for $f = f_R/2$, if the image series starts with a patterned state, say the Y state, successive frames exhibit Y and X stripes alternately. For $f = f_R/4$, the sequence of textures starting with the Y state in a series is Y-D-X-D-Y$\cdots$. Generally, for $f = f_R/(2n)$, the sequence is Y-(n–1)D-X$\cdots$, n being an integer and (n–1)D, the number of decay frames separating the Y and X textures. We have verified this up to $n = 32$. (b, column 4) Transient evolution of zigzag stripes oriented predominantly along y and occurring at polarity reversals of a square wave field in a 5-μm-thick nematic HOAB layer uniformly aligned along x; 114.7 °C, $f = 0.874$ Hz, $V = 5.1$ V; 2 μm each scale division. Frames F1–F3 are from time lapse recordings, with $T_F = 0.286$ s ($f_R = 3.496$ s^{-1}). Here $f = f_R/4$, so that the patterned states appear in alternate frames.

existence of the patterned state renders it difficult to ascertain the existence of a flow field. The distinguishing factors that indicate the origin of the instability relate to the pattern visibility in polarized light and the wave number dependence on voltage amplitude. From the absence of lens action for incident light vibrating along y, it is evident that only the polar angle of the director is modulated, while the azimuthal angle remains unchanged, as in the CH mode [12]. Secondly, we have verified that the wave number of the pattern is neither substantially nor systematically altered on increasing the control parameter; this rules out the BP or variable grating mode, which is characterized by a linear increase in the domain line density with bias voltage [5]. Adding to these, in planar untwisted cells of BEPC, PAA, and HOAB [Fig. 20(b)], we find the wave vector of the transient low frequency pattern to be along the initial director; we have reported earlier a similar observation for the transient stripes instability in 4-n-pentyloxyphenyl 4-n-decyloxybenzoate (10/5) [39]. From all these results, the instability in the TN case may be inferred as primarily the CH mode. The next question is that of its suppression until reaching high voltages in samples exposed to dc fields, and of its decay during constancy of square wave fields. We have recently discussed similar observations in planar nematic layers of 10/5 [39]. Essentially, under dc driving, the CH charge focusing is likely to be less effective because of unipolar charge carrier injection. The anisotropic electroconvection state is robust provided the CH term, approximately given by $-\alpha_2\tau_q\sigma_a[1 + q_c^2(\varepsilon_\parallel/\varepsilon_\perp) - (\varepsilon_a\sigma_\perp)/(\sigma_a\varepsilon_\perp)]$, is strong; here α_2 is a Leslie viscosity coefficient and q_c, the critical wave number in units of π/d [34]. It works out to be $\sim$0.8 N μs^2 S/m^3 for BEPC at 55 °C; by comparison, its value is $\sim$2.3 N μs^2 S/m^3 for the room-temperature nematic methoxybenzylidene butylaniline (MBBA) with the data from Ref. [33]. Therefore, the disruption of weak charge focusing in BEPC by charge injection under static or very low frequency fields is likely to suppress the instability until a sufficiently large voltage is applied to overcome it. As earlier noted, with the usual single coat of polyimide aligning layer, complete blocking of charge injection is not secured. This indicates porosity in the film, probably caused by impurities and rubbing.

From its field polarity dependence, the transient CH instability in BEPC may be taken as governed by flexoelectric polarization, in addition to conduction induced charge separation. In the total flexoelectric torque $\mathbf{\Gamma}_F$, as our results indicate, the component due to the field gradient $dE_z(t)/dz$ plays an important part in the evolution of periodic order. For specificity, consider the electric field distribution in the TN layer. For an applied dc voltage, when blocking layers prevent charge injection, voltage induced diffuse counterion layers contiguous to the electrodes modify the field so that it is homogeneous and diminished in bulk, but steeply increasing toward the electrodes in the Debye-like screening layers [40]. Selective adsorption of ions of the same sign at these layers results in enduring surface field asymmetry; differential mobility of the opposite charge carriers produces a transient surface field asymmetry [41]. When the blocking layers are imperfect, charge injection renders the surface field asymmetric while leaving the bulk field uniform [42]. Field polarity reversal disturbs the equilibrium field distribution in two important and time dependent ways. The bulk field rises suddenly and momentarily, as experimentally demonstrated in a study on transient dielectric response [43]. Secondly, field inhomogeneity extends into the bulk and, with passage of time, during the drift of counterion clouds, the inhomogeneity recedes toward the electrodes. These effects, which are particularly pronounced in the presence of intrinsic double layers as discussed previously [44], provide the condition suitable for the evolution of various transient instabilities. Thus, with thin samples of BEPC, we have previously observed [44] transient occurrence of homogeneous reorientation and interpreted it as the gradient flexoelectric analog of the usual Fréedericksz instability; well above threshold, this instability becomes patterned, showing extended domains along the easy axis. Further, in static fields, thin planar layers ($d \sim 8$ μm) have also been found to exhibit the BP instability.

The foregoing results suggest that in the steady voltage state of the driving square wave field, dE_z/dz and $\mathbf{\Gamma}_{GF}$, the

gradient flexoelectric torque, are 0 in the bulk. The absence of instability then implies a disruptive influence of charge injection on the CH charge focusing process, as earlier noted. However, consequent on polarity change, as argued above, field gradients that come to exist momentarily generate a nonzero $\mathbf{\Gamma}_{GF}$. If the sign of $\mathbf{\Gamma}_{GF}$ is such as to destabilize the planar state and support the CH process, bifurcation to the periodic state could occur. This situation, going by the results, is obtained near the negative electrode. Obviously, the signs of total flexocoefficient and field gradient are crucial for the choice between the electrodes. Needless to say that the transient effects in conducting nematics arise when the time τ_d for ion drift across the layer becomes comparable with the period of the exciting field. We may expect τ_d to be of the order of a few seconds, as discussed in Ref. [44]. In this interval, field configurational changes required for the $\mathbf{\Gamma}_{GF}$-stimulated CH instability may be obtained. Correspondingly, the transmitted light intensity variation due to the instability may last for a few seconds.

We may briefly compare our results with some of the recent findings [21,22] in planar samples subjected to very low frequency fields. In Phase 5, for $f = 30$ mHz or less, both CH and BP destabilizations occur separated in time and Fourier space, during each half cycle of the exciting sinusoidal field. However, in our experiments using square wave driving, only the CH mode is excited. Also in dc, Phase 5 shows the BP instability; here, at high voltages, the CH pattern is obtained. These differences may be attributed in part to the different waveforms employed in the two studies, i.e., square wave here and sine wave in Ref. [22]. In fact, at lower voltages, with a square wave, the bulk field may completely vanish in the steady state, but may increase to more than the applied voltage at polarity switchings when the ion transit time is smaller than the half period of the field. With a sine wave, the corresponding effects may become less severe, the extent of change depending on ion dynamics. Secondly, material parameters of significance to growth rates and thresholds of CH and BP instabilities could decide the appearance or otherwise of either instability; these parameters obviously vary for BEPC and Phase 5. The major difference between Phase 5 and BEPC results is with regard to the wave vector direction. In planar samples, it is not obvious as to where the maximum distortion develops. Experiments on TN Phase 5 will be interesting from this viewpoint.

Before concluding, while on the subject of convection rolls formed at the electrodes, we may mention two earlier observations for the sake of completeness. The first of these relates to "surface dielectric rolls" in a 90°-TN cell [45]; it has been demonstrated that, when the ratio of sample thickness to roll width is large, two systems of rolls form, each localized near a bounding surface and having its wave vector along the anchoring direction at this surface. Evidently, this instability is quite different from flexoelectrically assisted and polarity-sensitive conduction rolls discussed here. The second observation is that of two oppositely disposed oblique roll systems, each close to an electrode, in a pi-cell driven by low frequency (<30 Hz) fields [46]. This instability is conjectured to arise from the flexoelectric influence on EC, such as analyzed in Ref. [15], with opposite flexoelectric torques in the two half layers of the pi-cell causing opposite roll orientations. Clearly, this interpretation does not involve the dynamics of double-layer formation and transient evolution of the patterned state.

IV. CONCLUSIONS

The behavior of nematic fluids as weak electrolytes has important consequences to their dielectric, electroconvective, and flexoelectric responses. We have explored this aspect experimentally in a 90°-TN phenyl benzoate, employing square wave fields of various frequencies above 20 mHz. Of particular significance is the temporal evolution and decay of the CH instability in the very low frequency regime, below 2 Hz. We have characterized this effect by an analysis of optical response under varying conditions of temperature, applied bias, and frequency. This transient response is conditioned by temporal changes in the electric field pattern within the TN layer. In accounting for the suppression of periodic modulation under moderate applied voltages and steady field conditions, disruption of the CH process by charge carriers injected through porous aligning layers is envisaged. Likewise, momentary development of this modulation soon after polarity reversal is attributed to the gradient flexoelectric polarization assisted CH mechanism; spatial gradients of electric field, which are prominent near the electrode surfaces, render the quadrupolar flexoeffect active. Furthermore, the flexoelectric torque near the negative electrode is believed to be of the correct sign in enhancing the periodic charge separation effect due to conduction anisotropy. This would explain our main finding that the maximum distortion occurs close to the negative electrode. This assumes significance in the light of a recent report of low frequency temporal evolution of patterned instabilities having the largest distortion amplitude in the midplane of the layer [22]. We need to emphasize that the analysis in Ref. [22] is for symmetric boundary conditions, and situations in which electrical double-layer polarization and charge injection do not influence the instabilities. Further theoretical and experimental studies are necessary to evaluate the role of realistic boundary conditions, sample thickness, and electrical parameters of the material in determining the temporal behavior of competing instability modes.

ACKNOWLEDGMENTS

We thank Professor K. A. Suresh and Dr. Praveer Asthana for the experimental facilities. We are indebted to M/s Eastman Organic Chemicals for supplying, free of charge, the sample of BEPC used in this study.

[1] R. B. Meyer, Phys. Rev. Lett. **22**, 918 (1969).

[2] J. Prost and J. P. Marcerou, J. Phys. France **38**, 315 (1977).

[3] A. G. Petrov, in *Physical Properties of Liquid Crystals: Nematics*, edited by D. A. Dunmur, A. Fukuda, and G. R. Luckhurst (INSPEC-IEE, London, 2001).

[4] Y. P. Bobylev and S. A. Pikin, Sov. Phys. JETP **45**, 195 (1977).
[5] S. A. Pikin, *Structural Transformations in Liquid Crystals* (Gordon and Breach Science Publishers, New York, 1991).
[6] A. I. Derzhanski, A. G. Petrov, H. P. Hinov, and B. L. Markovski, Bulg. J. Phys. **1**, 165 (1974).
[7] A. I. Derzhanski and A. G. Petrov, Acta Phys. Pol. A **55**, 747 (1979).
[8] A. Derzhanski and A. G. Petrov, in *Advances in Liquid Crystal Research and Applications*, edited by L. Bata, Vol. 1 (Pergamon Press, Oxford, 1980).
[9] B. A. Umanskii, L. M. Blinov, and M. I. Barnik, Sov. Tech. Phys. Lett. **6**, 87 (1980).
[10] B. A. Umanskii, V. G. Chigrinov, L. M. Blinov, and Yu. B. Pod'yachev, Sov. Phys. JETP **54**, 694 (1981).
[11] H. P. Hinov, I. Bivas, M. D. Mitov, K. Shoumarov, and Y. Marinov, Liq. Cryst. **30**, 1293 (2003), and references therein.
[12] L. M. Blinov and V. G. Chigrinov, *Electrooptic Effects in Liquid Crystal Materials* (Springer, Berlin, 1994).
[13] A. Hertrich, A. P. Krekhov, and O. A. Scaldin, J. Phys. II France **4**, 239 (1994).
[14] S. Frunza, R. Moldovan, T. Beica, M. Giurgea, and D. N. Stoenescu, Europhys. Lett. **20**, 407 (1992).
[15] N. V. Madhusudana and V. A. Raghunathan, Liq. Cryst. **5**, 1789 (1989).
[16] W. Thom, W. Zimmermann, and L. Kramer, Liq. Cryst. **4**, 309 (1989).
[17] L. Kramer, E. Bodenschatz, W. Pesch, W. Thom, and W. Zimmermann, Liq. Cryst. **5**, 699 (1989).
[18] T. Tóth-Katona, N. Éber, Á. Buka, and A. Krekhov, Phys. Rev. E **78**, 036306 (2008).
[19] A. Krekhov, W. Pesch, N. Éber, T. Tóth-Katona, and Á. Buka, Phys. Rev. E **77**, 021705 (2008).
[20] A. Krekhov, W. Pesch, and Á. Buka, Phys. Rev. E **83**, 051706 (2011).
[21] N. Éber, P. Salamon, and Á. Buka, in *Proceedings of the 13th Small Triangle Meeting on Theoretical Physics*, edited by J. Buša, M. Hnatič, and P. Kopčanský (IEP SAS, Košice, 2012), p. 56.
[22] N. Éber, L. O. Palomares, P. Salamon, A. Krekhov, and Á. Buka, Phys. Rev. E **86**, 021702 (2012).
[23] W. H. de Jeu and Th. W. Lathouwers, Mol. Cryst. Liq. Cryst. **26**, 225 (1974).
[24] D. Balzarini and P. Palffy-Muhoray, in *Liquid Crystals and Ordered Fluids*, edited by A. C. Griffin and J. F. Johnson, Vol. 4 (Plenum Press, New York, 1984).
[25] P. Kumar and K. S. Krishnamurthy, Phys. Rev. E **74**, 031705 (2006).
[26] H. Gruler and L. Cheung, J. Appl. Phys. **46**, 5097 (1975).
[27] R. N. Thurston, J. Appl. Phys. **55**, 4154 (1984).
[28] G. Barbero and G. Durand, J. Phys. France **51**, 281 (1990).
[29] G. Barbero, L. R. Evangelista, and N. V. Madhusudana, Eur. Phys. J. B **1**, 327 (1998).
[30] G. Derfel and M. Buczkowska, Opto-Electron. Rev. **19**, 66 (2011).
[31] C. V. Brown and N. J. Mottram, Phys. Rev. E **68**, 031702 (2003).
[32] P. G. de Gennes and J. Prost, *The Physics of Liquid Crystals*, 2nd ed. (Clarendon Press, Oxford, 1993).
[33] E. Bodenschatz, W. Zimmermann, and L. Kramer, J. Phys. France **49**, 1875 (1988).
[34] L. Kramer and W. Pesch, in *Pattern Formation in Liquid Crystals*, edited by Á. Buka and L. Kramer (Springer, Berlin, 1996).
[35] R. Williams, J. Chem. Phys. **39**, 384 (1963).
[36] B. Dressel and W. Pesch, Phys. Rev. E **67**, 031707 (2003).
[37] K. S. Krishnamurthy, Mol. Cryst. Liq. Cryst. **133**, 1 (1986).
[38] C. Z. Van Doorn, J. Phys. **36**, C1-261 (1975); J. Appl. Phys. **46**, 3738 (1975); **46**, 3746 (1975).
[39] K. S. Krishnamurthy and P. Kumar, Phys. Rev. E **76**, 051705 (2007).
[40] G. Barbero, D. Olivero, N. Scaramuzza, G. Strangi, and C. Versace, Phys. Rev. E **69**, 021713 (2004).
[41] R. N. Thurston, J. Cheng, R. B. Meyer, and G. D. Boyd, J. Appl. Phys. **56**, 263 (1984).
[42] S. Lu and D. Jones, Appl. Phys. Lett. **16**, 484 (1970).
[43] M. Scalerandi, P. Pagliusi, G. Cipparrone, and G. Barbero, Phys. Rev. E **69**, 051708 (2004).
[44] K. S. Krishnamurthy and P. Kumar, Liq. Cryst. **34**, 257 (2007).
[45] H. Bohatsch and R. Stannarius, Phys. Rev. E **60**, 5591 (1999).
[46] Y. Xiang, Y. K. Liu, X. S. Xie, J. M. Li, J. H. Wang, and Z. G. Cai, Appl. Phys. Lett. **97**, 203507 (2010).